TIME-RESOLVED REMOTE RAMAN SPECTROSCOPY FOR VENUS EXPLORATION

S. K. Sharma[1], A. K. Misra[1] and T. E. Acosta[1], M. D. Dyar[2], S. M. Clegg[3] and R. C. Wiens[3]

[1]Hawaii Institute of Geophysics and Planetology, University of Hawaii, 1680 East-West Rd., POST #602 Honolulu, HI, 96822, sksharma@soest.hawaii.edu

[2]Dept. of Astronomy, Mt. Holyoke College, South Hadley, MA 01075, mdyar@mtholyoke.edu [3]Los Alamos National Laboratory, P.O. Box 1663 MS J565, Los Alamos, NM 87545, sclegg@lanl.gov

Introduction:

Time-resolved (TR) remote Raman spectroscopy (RS) is being develpoed for flight as a part of SuperCam instrument for Mars 2020 Rover Mission, and has been proposed as a mineralogical analysis system for Venus' Surface and Atmosphere Geochemical Explorer (SAGE) Mission [1, 2]. Raman spectroscopy has several distinct advantages over other spectroscopic techniques that have been used in the past missions, specifically including the capability for rapid mineralogical analysis at standoff distances [e.g., 3-5]. In some cases planetary minerals and rocks containing transition-metal and rare-earth ions produce a strong fluorescence when excited with UV and visible lasers overlaping with minerals' Raman spectra [e.g., 6]. However, the fluorescence decay time or lifetime of transition metal ions and rare-earth ions in minerals and rocks is much longer (μs to ms) than the lifetime of the Raman signals (~10^{-13} s) [e.g., 7]. Therefore time-resolved (TR) Raman spectroscopy exploits the short lifetime of the Raman signal of minerals to identify these materials on planetary surfaces during daytime or nighttime without interfering fluorescence. Raman spectroscopy has been used successfully to investigate spectra of minerals at high temperatures and pressures [e.g., 8], and has been demonstrated in the laboratory for detecting minerals under high P and T conditions relevant to Venus exploration [9, 10]. We describe here a compact gatable planetary Raman spectrograph (PRS) developed at the University of Hawaii (UH), characterize Raman spectra of several minerals species suggested to be present on Venus surface, and show detection limits in mixtures in a basalt glass analog with a 532-nm laser excitation.

Samples:

Starting samples were chosen based on work that builds upon results from the Vega and Venera landers. Those three sets of XRF major element analyses from the surface of Venus all suggest the presence of basaltic rock types along with variable amounts of S, either primary or secondary from atmospheric interactions. The most common models predict that the surface of Venus is rich in the mineral wollastonite or the assemblage calcite + quartz, depending on elevation and temperature [e.g., 11-14]. These models also predict that the iron minerals hematite or magnetite will be present.

The most well-known atmosphere surface reaction for Venus is the so-called Urey equilibrium [11-13],

$CaSiO_3 + CO_2 = CaCO_3 + SiO_2$ ....[1]
(wollastonite) (calcite) (silica)

This reaction is near equilibrium at the Venus surface temperature and CO_2 pressure, and so could buffer CO_2 pressure.

Other workers [15-17] used thermochemical modeling to predict chemical weathering reactions between basalt and a CO_2 and SO_2-rich atmosphere. Abundances of sulfur-bearing gases (SO_2, OCS, H_2S, etc.) are second only to that of CO_2 in the Venus atmosphere, and are likely to be important weathering agents at the Venus surface.

Other predictions of Venus surface mineralogy come from Burns and Straub [18-19], who used observed emissivity to infer the presence of magnetite, hematite, Fe-sulfides, olivine, amphibole, micas, and ilvaite ($CaFe^{2+}Fe^{3+}{}_2(SiO_4)_2(OH)$). From these models, we selected a set of seven minerals for use in creating fine-grained mechanical mixtures of varying amounts of minerals and glasses likely to be present on Venus surface (Table 1). We then created mixtures of these rock-forming minerals with the synthetic Fe-containing glass, using 1, 3, and 10 % by volume of each mineral [20]. Fine grain mixtures of glass and various minerals were pressed to form a 12.5 mm disk and used for Raman measurements.

Table 1. Samples Studied

	Pure Minerals Used in mixtures
Anh	Anhydrite (sulfate)
Pyx	Diopside (pyroxene)
Ap	Chlorapatite (phosphate)
Plg	Plagioclase
Ol	Olivine
Qtz	Quartz
Cal	Calcite

Mixtures (% are by mineral mode, or vol %)

Sample No.	Anh	Pyx	Ap	Plg	Ol	Qtz	Cal
#1	1	1		1	1	1	
#2		3					
#3		1					
#4	1			1		1	
#5	3	3		3	3	3	
#6	1		1	1			
#7	3		3	3			
#8	3			3			3
#9		10					
#10	10	10					
#11	10	10		10	10		
#12	10		10	10			
#13	10	10		10	10	10	
#14	10			10		10	
#15						10	
#16		10			10	10	
#17				10		10	
#18			10			10	10
D.L.*	1	≥10	1	3	1	1	3

* Detection limit (%)

Experimental Setup:

Figure 1 shows the photograph of the planetary Raman spectrograph (PRS) used with a 532-nm pulsed laser source. The remote Raman system uses the compact Raman spectrograph with dimension 10 cm (length) x 8.2 cm (width) x 5.2 cm (high). The spectrograph was constructed using a custom volume holographic HoloPlex grating from Kaiser Optical System Inc. (Ann Arbor, MI, USA). The spectrograph is equipped with a custom gatable thermo-electrically cooled mini-intensified charge coupled device (mini-ICCD) camera. Spectral coverage is from 90 to 4520 cm^{-1}; Stokes-Raman shifted from 532 nm laser excitation. The spectrograph is also capable of collecting time-resolved laser-induced breakdown spectra and laser-induced native fluorescence (LINF) of minerals and rocks in the wavelength rage 534-700 nm [21-22].

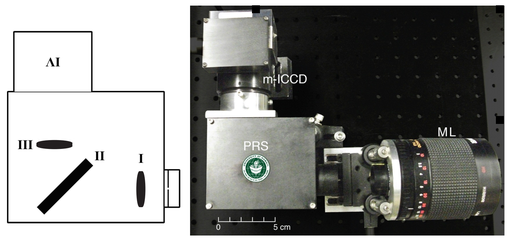

Figure 1. Photograph of the Planetary Raman and LINF system with a 7.6-cm diameter mirror (ML) camera lens as collection optics and compact spectrograph with custom mini-ICCD camera (m-ICCD). Schematic diagram of the spectrometer is shown on the left with parts labeled (see text).

The F/2 spectrometer is schematically shown to the left of the photograph in Fig.1. There are two lenses (I and III) and two stacked volume phase holographic (VPH) transmission gratings (Kaiser HoloPlex VPH grating) (II). The VPH gratings are inside the two quartz plates, only angled differently to produce two images on m-ICCD camera with different spectral ranges. When light from the target passes into the system through the slit and is collimated by the first lens (I), the light is split by the grating into two halves (top and bottom) as well as into its spectral components along the x axis and turned 90°. The second lens focuses the collimated dispersed light onto the mini-ICCD (IV). The mini-ICCD has a CCD chip 1392x1040 pixels with pixel size 6.45 μm². The major advantages of this spectrometer include its small size, the small number of optical components yielding the greatest throughput of signal, and direct coupling allowing for the preservation of the vertical image orientation from the target. With 50 μm slit the resolution of the spectrograph is ~15 cm^{-1} (0.43 nm) in the 100-2400 cm^{-1} and ~13 cm^{-1} (0.37 nm) in 2400-4500 cm^{-1} region.

The weight of the compact spectrograph built with aluminum is 571 g and that of the mini-ICCD detector is 620 g. The weight of the PRS system is much less as compared to the commercial Kaiser Optical System's HoloSpec spectrograph and Princeton Instrument's ICCD detector (PI-IMAX2) weighing 5 and 4.1 kg, respectively.

Standoff Raman experiments employed a Nd:YAG frequency doubled pulse laser operating at 15 Hz and with a maximum pulse energy of 17 mJ/pulse at 532 nm. The pulse width of the laser pulses was 10 ns. A 10x beam expander was used to focus the 532 nm laser beams collinear with the telescope's optical axis to 5-mm diameter spot onto the sample located at 2-m from the system in the air. A SuperNotch filter was used to block the 532-nm Rayleigh scattered light from reaching the spectrograph.

Results:

Figure 2(a) shows the stand-off Raman spectra at 2-m distance recorded from 12.5-mm disks of pressed powdered minerals: anhydrite (Anh), chlorapatite (Ap) and α-quartz (Qtz). Figure 2(b) illustrates the stand-off Raman spectra of olivine (Ol), pyroxene (Pyx), plagioclase (Plg), and α-quartz (Qtz). The positions of the strong "Raman fingerprint" lines of these minerals are listed in Table 2.

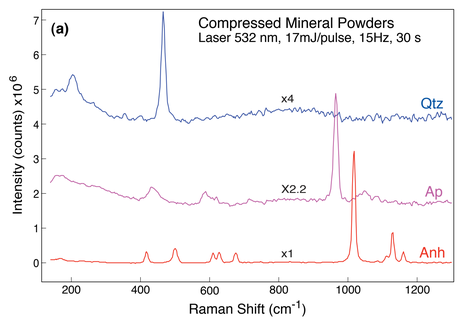

Figure 2 (a). Stand-off Raman spectra in air of anhydrite (Anh), chlorapatite (Ap) and α-quartz (Qtz) at 2-m distance.

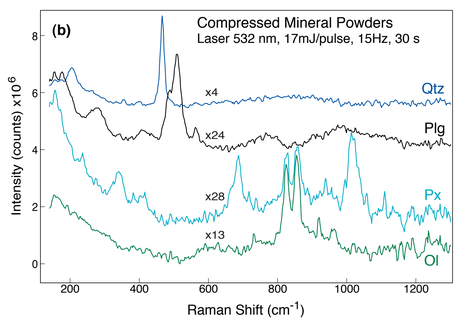

Figure 2(b). Stand-off Raman spectra in air of olivine (Ol), pyroxene (Pyx), plagioclase (Plg), and α-quartz (Qtz) at 2-m distance.

The spectra of minerals [Figs. 2 (a) and (b)] are normalized such that the intensities of the Raman fingerprint lines of individual minerals are the same as the strong 1018 cm^{-1} line of Anh. In the spectra of these minerals, the strongest Raman line of symmetric stretch of SO_4 ions in anhydrite appear at 1018 cm^{-1}, and the weakest Raman fingerprints are those of Pyx and Plg. Relative Raman cross section of the fingerprint Raman lines of various minerals can be estimated by the inverse of the multiplication factor in Fig. 2a and 2b. In the spectrum of pyroxene (Pyx) the Raman lines of pyroxene appear at 664 (sh), 686 and 1012 cm^{-1} and a fingerprint doublet of olivine (826 and 857 cm^{-1}) is also observed. The presence of a doublet in the ν_s(Si-O-Si) of pyroxene spectrum indicate that ortho-pyroxene is present in the sample, and the olivine doublet indicate that ~13 vol % of olivine powder is in the sample (see Table 2).

Table 2. Raman fingerprint lines of various minerals

Mineral	Raman Fingerprints (cm^{-1})	Assignments
Anhydrite (Anh)	1018	$\nu_s(SO_4)$
Pyroxene (Pyx)	664 (sh), 686	ν_s(Si-O-Si)
	1012	ν_s(Si-O(NBO*))
Olivine (present in Pyx sample)	826, 857	$\nu_1+\nu_3(SiO_4)$
Chlorapatite (Ap)	964	$\nu_s(PO_4)$
Plagioclase (Plg)	488, 507	$\nu_s(TO_4)$ four-membered rings of TO_4 tetrahedra, T = Si, Al
Olivine (Ol)	824, 854	$\nu_1+\nu_3(SiO_4)$
α-Quartz (Qtz)	204	Lattice mode
	465	ν_s(Si-O-Si) six-membered rings of SiO_4 tetrahedra

*NBO = Non-bridging oxygen

Standoff Raman spectra, at 2-m distance, of the glasses containing 1, 3 and 10 wt% of anhydrite with other minerals are shown in Fig. 3.

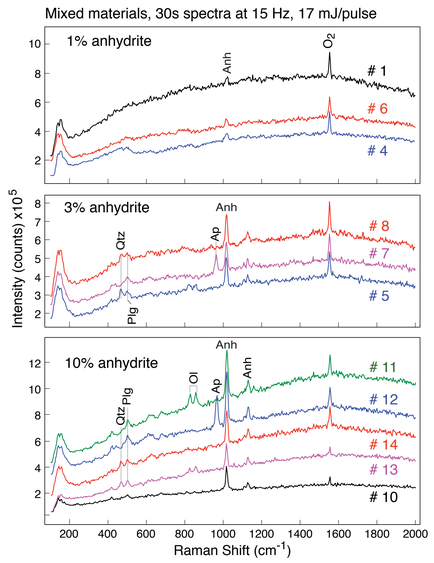

Figure 3. Stand-off Raman spectra of the glass samples containing 1, 3 and 10 vol % of anhydrite (Anh) with other minerals as marked at 2-m distance

The symmetric stretching mode, $\nu_s(SO_4)$, in anhydrite appears at 1018 cm^{-1} in the spectra of sample containing 1, 3 and 10 wt% anhydrite in the basaltic glass matrix. In the samples containing 3 and 10 wt% Anh weak antisymmetric stretching modes, $\nu_{as}(SO_4)$, at ~1112 and 1128 cm^{-1} are also observed. In Figs. 2a, and 2b, in addition to the 1018 cm^{-1} Anh Raman line, the fingerprint Raman lines are also observed for Qtz (465 cm^{-1}); Plg (doublet 488 and 507 cm^{-1}); olivine (doublet 824 and 854 cm^{-1}); and Ap (964 cm^{-1}).

Standoff Raman spectra at 2-m distance of olivine containing mixed minerals in the basaltic glass matrix with various other minerals are shown in Fig. 4. The fingerprint doublet of olivine at 824 and 854 cm^{-1} is clearly visible above the fluorescence background. In addition, the Raman fingerprints of Anh, Plg, Pyx, Qtz and of the atmospheric molecular oxygen at 1554 cm^{-1} are also observed at their respective positions (Table 2). The observed broad fluorescence background in these spectra must have lifetime shorter than 100 ns, the gate used for measuring these spectra, and it most likely has biogenic in origin.

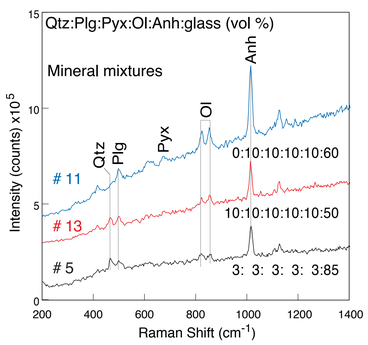

Figure 4. Stand-off Raman spectra at 2-m of olivine with various other minerals in the glass matrix as marked. Spectra are vertically spaced for clarity.

Figures 5 and 6 illustrate stand-off Raman spectra at 2-m distance of samples # 9 to #13 and # 14 to #18 in the glass matrices (see Table 1), respectively.

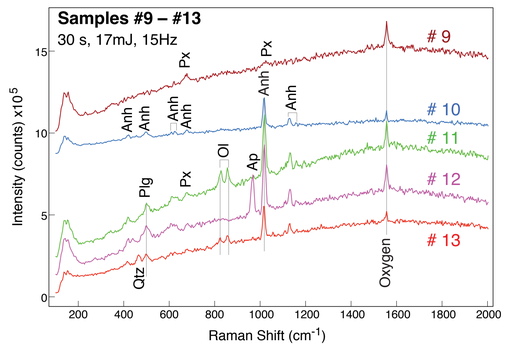

Figure 5. Stand-off Raman spectra at 2-m of samples # 9 – # 13 mixed minerals in the glass samples with 10 vol % of various minerals (see Table 1) as marked. Spectra are vertically spaced for clarity.

In the spectrum of sample #9 that contains 10 vol % diopside pyroxene, the weak Raman lines marked by Pyx at 666 and 1012 cm^{-1} are also observed (Fig. 5). In the sample containing anhydrite, the 1012 cm^{-1} Raman line of the Pyx is partially masked by the strong line of anhydrite at 1018 cm^{-1}. In the Raman spectrum of the sample # 18 in Fig. 6, a strong Raman line of symmetrical stretching mode of carbonate ions, ($\nu_1(CO_3)$), at 1084 cm^{-1} is detected. The weak Raman lines of calcite at 714 cm^{-1} ($\nu_4(CO_3)$), and a lattice mode of calcite at 285 cm^{-1} are also observed.

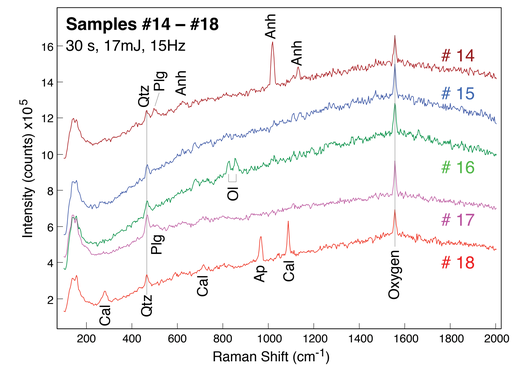

Figure 6. Stand-off Raman spectra at 2-m of samples #14 – #18 of mixed minerals in the glass matrix with 10 vol % of various minerals (see Table 1) as marked. Spectra are vertically spaced for clarity.

It is known that the relative Raman efficiencies of the various minerals vary with mineral species [23], and also show dependence on grain orientation [24] and particle size [25]. The detection limits of various minerals observed in the present work are summarized in Table 1. The detection limits of Anh, Ap, Ol and Qtz are 1 vol % in the glass matrix. The calcite and plagioclase were detected at 3 vol % concentrations. The pyroxene fine-grained crystals, which have lowest Raman efficiencies, were detected at ≥ 10 wt% concentration in the basalt glass matrix.

Summary:

The Raman data presented here show the ability of the compact gatable planetary Raman spectrograph system with pulse laser excitation to detect low concentrations of fine-grained mixed multiple minerals. The Raman system will detect various minerals simultaneously within a 5-mm diameter circle in a strongly absorbing matrix such as basaltic glass. A standoff Raman instrument would be capable of making about one thousand mineralogical observations of surface samples within a two hour surface mission. For the mineral studies, a gated remote Raman system will be very useful for future Venus Missions involving landers.

Acknowledgements:

The authors would like to thank Dr. Jennifer Fine for providing synthetic volcanic glass. At the University of Hawaii, fabrication of the compact Raman spectrograph has been supported in part by NASA MIDDP grant NNX08AR10G.

References:

[1] Clegg, S.M. et al. (2014) *Appl. Spectrosc.* **68**, 925-936.
[2] Clegg, S.M. et al. (2015) *LPSC*, **46**, abstract #472.
[3] Sharma, S.K. et al. (2010) *Proc. SPIE*, **7691**, 76910F/1- 76910F/11 (2010).
[4] Misra, A.K. et al. (2011) *Appl. Spectrosc.* **66**, 1279-1285.
[5] Abedin, M.N. et al. (2013) *Appl. Optics*, **52**, 3124-3126.
[6] Misra, A.K. et al. (2005) *Spectrochim Acta* A, **61**, 2281-2287.
[7] Gaft, M., Reisfeld, R. and Panczer, G. (2005) *Luminescence Spectroscopy of Minerals*, pp. 356, Springer-verlag, New York.
[8] Sharma, S. K. (1989) *Vib. Spectra Struct.* **17B**, 513 568.
[9] Sharma, S.K. et al. (2011) *Proc. Trans. Royal Soc.* A **368**, 3167-3191.
[10] Sharma et al. (2011) *Spectrochim. Acta*, A **80**, 75– 81.
[11] Lewis, J.S. and F.A. Kreimendahl (2008) *Icarus*, **42**, 330-337.
[12] Fegley, Jr, B. and R.G. Prinn (1989) *Nature*, **337**, 55-58.
[13] Fegley B. Jr. et al. (1992) Proc. LPSC, **22**, 3-19.;
[14] Johnson, N. M. and Fegley, B. (2000) *Icarus*, **146**, 301-306.
[15] Zolotov M.Y. et al. (1997) Icarus, **130**, 475-494.
[16] Treiman A. and S.P. Schwenzer (2009) *Venus Geochemistry: Progress, Prospects, and New Missions*, Abstr. # 2011.
[17] Treiman, A. (2010) *International Venus Conference, Aussois 2010*, Abstr. # 05-02.
[18] Burns R.G. and Straub, D.W. (1992) *Intern. Colloq. Venus, LPI Contrib. No. 789.*
[19] Burns R.G. and Straub, D.W. (1993) *LPSC XXIV*, 233-234.
[20] Sharma, S. K. et al. (2011) *LPSC*, **42**, abstract #1250.
[21] Sharma, S. K. (2014) PLANEX, **4**, no. 4, 26-29. http://www.prl.res.in/~rajiv/planexnews/oldPlanexpdf/Volume%20-4,%20Issue-4.pdf
[22] Gasda, P.J. et al. (2015) *Appl. Spectrosc.* **69**, 173-192.
[23] Stoper, J.D. et al. (2005) Spectrochim Acta A, **61**, 2315-2323.
[24] Wang, A. et al. (1995), *J. Geophys. Res. Planets*, **100**, 21189–21199.
[25] Chio, C.H. et al. (2003) *Appl. Spectrosc.*, **57**, 774-783.

HIGP Hawai'i Institute of Geophysics & Planetology
soest
MOUNT HOLYOKE
Los Alamos NATIONAL LABORATORY EST. 1943
NASA